Cermets based on new submicron Ti(C,N) powder: microstructural development during sintering and mechanical properties

Journal:	*International Conference on Sintering 2011*
Manuscript ID:	P_04_1037.R1
Symposium:	04:Microstructural evolution in sintering processes
Date Submitted by the Author:	03-May-2012
Complete List of Authors:	Veitsch, Christopher; Treibacher Industrie AG, R&D non oxide ceramics

Cermets based on new submicron Ti(C,N) powder: microstructural development during sintering and mechanical properties

A. Demoly[1], C. Veitsch[2], W. Lengauer[1], K. Rabitsch[2]

[1]Vienna University of Technology, Vienna, Austria.
[2]Treibacher Industrie AG, Althofen, Austria.

ABSTRACT

Ti(C,N) cermets based on a newly developed submicron Ti(C,N) grade (FSSS ≈0.7µm) were compared to cermets based on standard Ti(C,N) (FSSS ≈1µm) having the same C/N ratio. Sintering of the cermet green bodies was carried out under vacuum conditions (< 1 bar), partly under nitrogen atmosphere. In order to get insight into the development of the microstructure (i.e. phase formation and evolution during sintering, porosity), the sintering process was interrupted at specific temperatures (1175, 1300, 1400 and 1460°C, respectively) by fast cooling. The changes in the microstructure were monitored by XRD, SEM, light-optical microscopy and magnetic properties. XRD analysis shows the total dissolution of the (Ta,Nb)C and WC during heating and the formation of three fcc phases at the end of the sintering cycle. One corresponds to the binder phase, the second can be assigned to the rim phase and exhibits a complex solid solution (Ti,Ta,Nb,W)(C,N) and the third to undissolved Ti(C,N) cores. The small difference in the Ti(C,N) starting powder grain size was found to have a significant impact on the microstructure. The submicron powder shows higher activity upon sintering, therefore, a larger amount of rim phase and a further dissolution of the Ti(C,N)-rich cores are observed. The microstructural changes induced by using submicron Ti(C,N) cause higher magnetic specific saturation ($4\pi\sigma$), coercive force (HcJ) and hardness (HV10), whereas the Palmqvist fracture toughness (K_{IC}) decreases slightly.

INTRODUCTION

The microstructure of Ti(C,N)-based cermets is typically characterised by a core-rim structure. The rim is composed of an inner and an outer part, which are formed during solid-state and liquid-phase sintering, respectively. In Ti(C,N)-based cermets the cores stem from the undissolved Ti(C,N) particles, while an homogenised carbonitride phase forms the rim. The main parameter controlling the microstructure formation is the diffusion of the elements. Therefore, using smaller starting Ti(C,N) particle size may lead to a significant modification of the microstructure and thus of the properties of cermets[1].

The present study compares the development of the cermet microstructures during sintering using interruption of the sintering process and characterization by SEM, XRD as well as magnetic properties measurements. Two powders were used, the first is a conventional fine Ti(C,N) powder the second a newly developed submicron Ti(C,N) powder.

EXPERIMENTAL

The chosen material specifications belong to the material class HT-P10 (ISO513 1992-06), which contains a large amount of Ti(C,N) and has a low content of other carbides. This application class fits particularly for the machining of steel and cast steel with high cutting speed and low feed rate.

Starting materials

The cermets' composition is listed in Table I, while the properties of the individual powders are listed in Table II. Two Ti(C,N) powder grades – a conventional Ti(C,N) powder (FSSS = 1µm) and a submicron Ti(C,N) powder (FSSS = 0.7µm) – both with a [C]/([C]+[N]) ratio of 0.5 – were used to prepare cermet mixtures (Table II, Figure 2). Both Ti(C,N)-grades as well as the other carbides are industrial grades by Treibacher Industrie AG. Figure 1 shows a SEM image of the Ti(C,N) powders. The binder powders Co and Ni were supplied by Umicore and Inco, respectively.
The grain size was determined using the Fischer Sub Sieve Sizer (FSSS) (Table II) and diffraction laser particle size analyser (Figure 2). The O, C and N contents were measured by carrier gas hot extraction.

Table I. Composition of the cermets I and II

		fine Ti(C,N)	submicron Ti(C,N)	(Ta,Nb)C	WC	Cr_3C_2	Co	Ni
Grade A	I (wt%)	59	-	10	16	1	6.5	6.5
	II (wt%)	-	59	10	16	1	6.5	6.5

Table II. Properties of the individual powders

	fine Ti(C,N)	submicron Ti(C,N)	(Ta,Nb)C	WC	Cr_3C_2	Co	Ni
Carbon (wt%)	10.59	10.75	8.10	6.17	13.22	0.15	0.13
Nitrogen (wt%)	10.79	10.60	0.01	-	0.02	-	-
Oxygen (wt%)	0.59	1.08	0.24	0.19	0.53	0.55	0.05
Grain size (FSSS in µm)	1.0	0.7	1.3	0.6	1.9	0.9	1.3

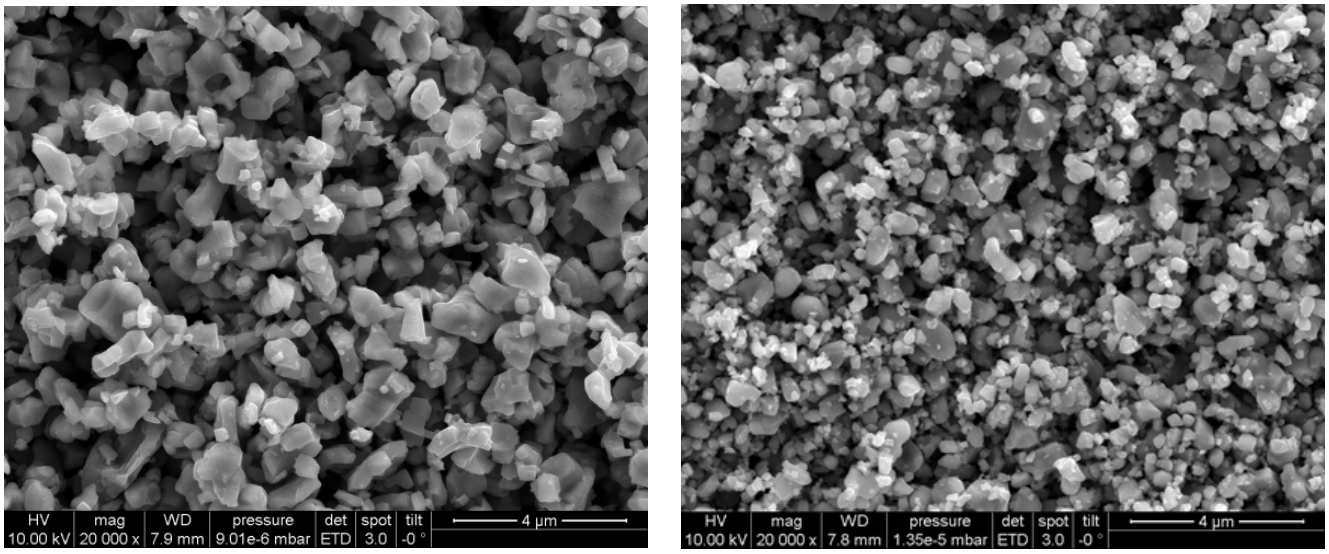

Figure 1. Ti(C,N) powders, conventional (left) and submicron (right), SEM, SE, 20000x

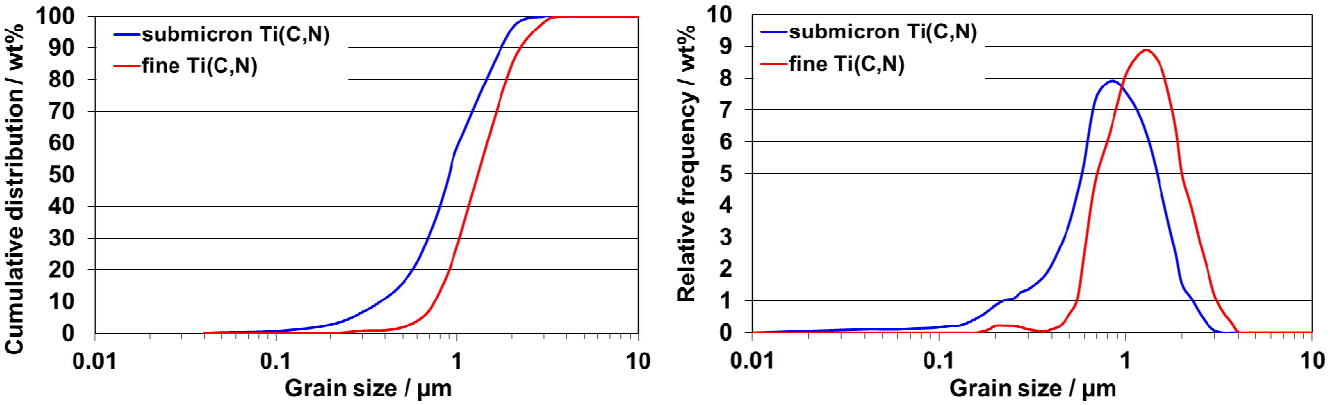

Figure 2. Ti(C,N) powders, cumulative (left) and differential (right) grain size distribution

Preparation of green bodies

After weighing the powders, the blends were mixed and milled for 72h in a ball-mill filled with hardmetal balls and cyclohexane. The obtained cermet powders were dried and agglomerated and then pressed with 150MPa to cylindrical bodies (8mm height and 12mm in diameter) in an uniaxial press.

Dilatometry

The shrinkage of the samples was investigated by dilatometry (DIL801, Bähr-Thermoanalyse GmbH) following the sintering profile depicted in Figure 3 but under vacuum and with slightly shorter dwell times.

Sintering

The samples were placed in a graphite crucible and sintered in an induction furnace first under vacuum and then under nitrogen atmosphere (Figure 3). The sintering process was interrupted by fast cooling at 1175°C, 1300°C, 1400°C and 1460°C, respectively, after different dwell times (Figure 3, Table III) allowing a chronological observation of the microstructure evolution, phase formation and of the magnetic properties. After interrupting the sintering process, XRD, light-optical microscopy (LOM) and scanning electron microscopy (SEM) were applied to assess the formed phases. Furthermore, light optical microscopy (LOM) images were made with an inverted reflected light microscope (Olympus Co.), and image analysis with the program AnalySIS Ver. 5.0. The polished samples were etched using an basic oxide polishing silicate suspension to remove the binder and to obtain an higher contrast of the grain boundaries. A scanning electron microscope (FEI Quanta 200FEG) using a back scattered electron filter was employed to inspect the microstructure as well as the grain size of the cermets. The calculation of the core-to-rim ratio was made using the program ImageJ 1.43u on basis of the grey scale difference between core (dark) and rim (bright). The coercive force (HcJ) and the weight specific magnetic saturation ($4\pi\sigma$) were measured using a Koerzimat CS 1.096 (Förster). After final sintering the hardness (HV10) and fracture toughness (K_{IC}) of the samples were measured using the Shetty equation.

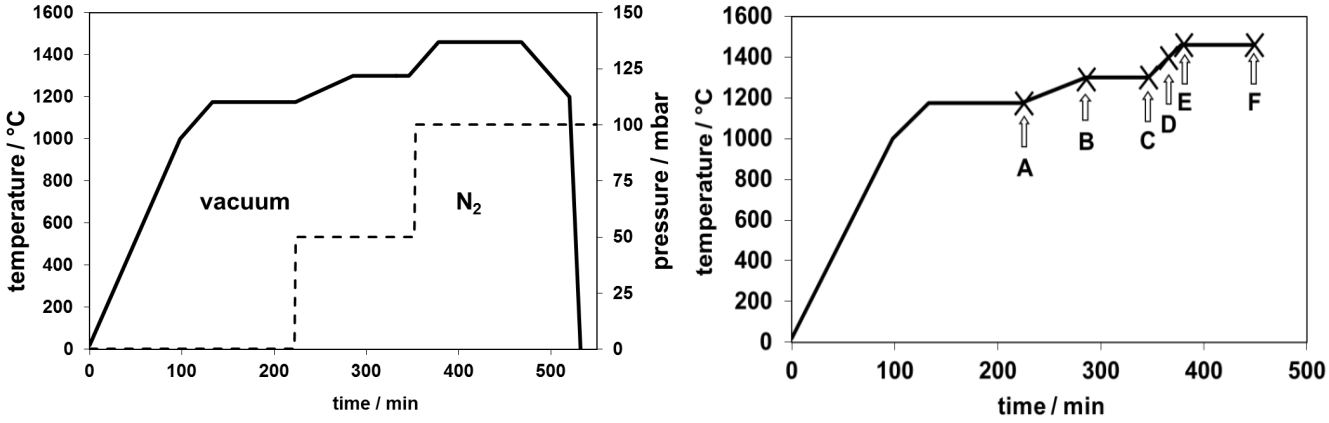

Figure 3. Sintering profile (left) and sintering interruption points (right)

Table III. Sintering interruption points

	A	B	C	D	E	F
Temperature in °C	1175	1300	1300	1400	1460	1460
Time in min	90	0	60	0	0	90

RESULTS

Dilatometry

The shrinkage curves show a higher shrinkage for cermet II with submicron Ti(C,N) from the beginning of the first dwell up to the formation of the liquid phase, during the third dwell. The solid-state sintering is obviously further advanced for cermet II with submicron Ti(C,N) than for cermet I with fine Ti(C,N). Generally, the beginning of the shrinkage correlates with the rearrangement of powder particles. The introduction of finer Ti(C,N) powder in cermet II causes faster diffusion and therefore, higher shrinkage from 1175°C up to around 1400°C (appearance of the liquid phase). The formation of the liquid phase at 1400° marks the end of the solid-state sintering regime and the balancing of the shrinkage for both cermets.

The total shrinkage (Table IV) as well as the shrinkage rate (Figure 4) are identical for both cermets and therefore, independent of the grain size of the used Ti(C,N) powder. In addition, the temperature of the shrinkage rate maximum is almost identical for both cermet grades (Table IV).

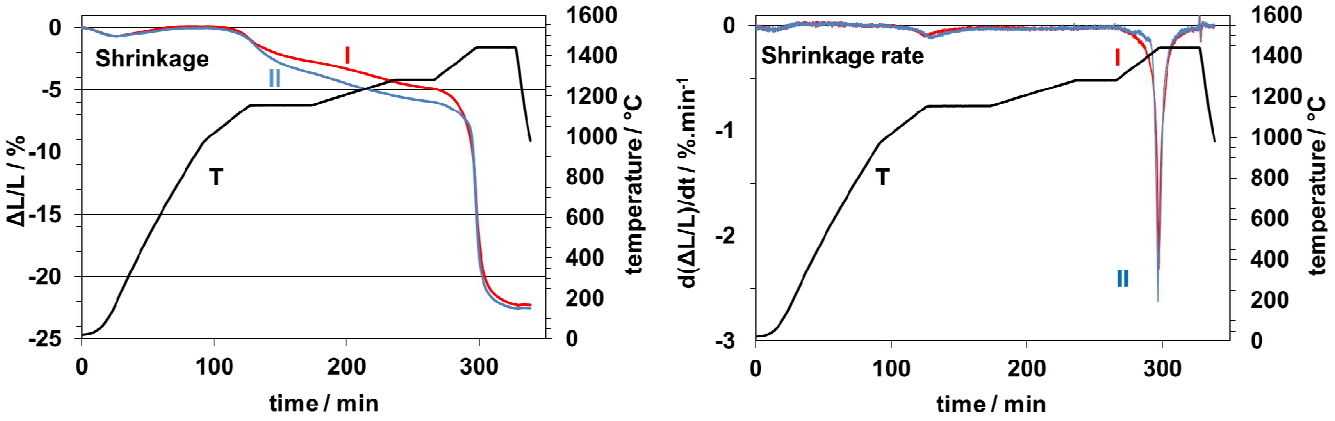

Figure 4. Shrinkage (left) and shrinkage rate (right) of cermets I and II

Table IV. Shrinkage rate and overall shrinkage of cermets I (with fine Ti(C,N) and II (with submicron Ti(C,N))

Cermet	Main shrinkage rate maximum °C	Total shrinkage %
I	1425	22.3
II	1426	22.6

Apparent porosity - light optical microscopy (LOM)

The evolution of the microstructure during the sintering process of stages C to F is shown in Figure 5 and 6 (for porosity quantification of all stages and SEM analysis see below). During heating from 1175°C to 1300°C homogenisation occurs alongside the formation of new phases. At stage C (1300°C – 60 min) no large difference between the two cermet grades can be observed. A large amount of rim phase had formed and the porosity had further declined. At 1400°C (stage D), a dramatic modification of the porosity is observed. Cermet I with fine Ti(C,N) shows fewer but larger irregular pores whereas cermet II with submicron Ti(C,N) has many and much smaller pores with rounded shape. This pore structure continues to stage E (1460°C – 0 min), however, with a significant drop in apparent porosity. Finally, the porosity disappears completely during liquid-phase sintering at 1460°C between E (0 min) and F (90 min) in both grades. In Figure 7, the porosity surface area (from image analysis) of both samples is presented for all stages. Cermet II with submicron Ti(C,N) exhibits a lower porosity than cermet I between 1175°C (A) and 1400°C (D). Obviously, the densification of cermet II takes largely place between 1175°C (A: 33%) and 1300°C (B: 9%), whereas for cermet I with fine Ti(C,N) the densification needs longer and higher temperatures. The porosity of cermet I after 90 min dwell time at 1300°C (C: 12%) is still slightly higher than that of cermet II at 1300°C without dwell time (B: 9%). During the dwell time at 1300°C (B-C) the porosity of sample II decreases slightly from 9 to 7%, while the porosity of cermet I decreases dramatically from 27 to 12%. Above 1400°C (D), the porosity of both cermets is nearly the same and full densification is achieved at 1460°C after 90 min (F).

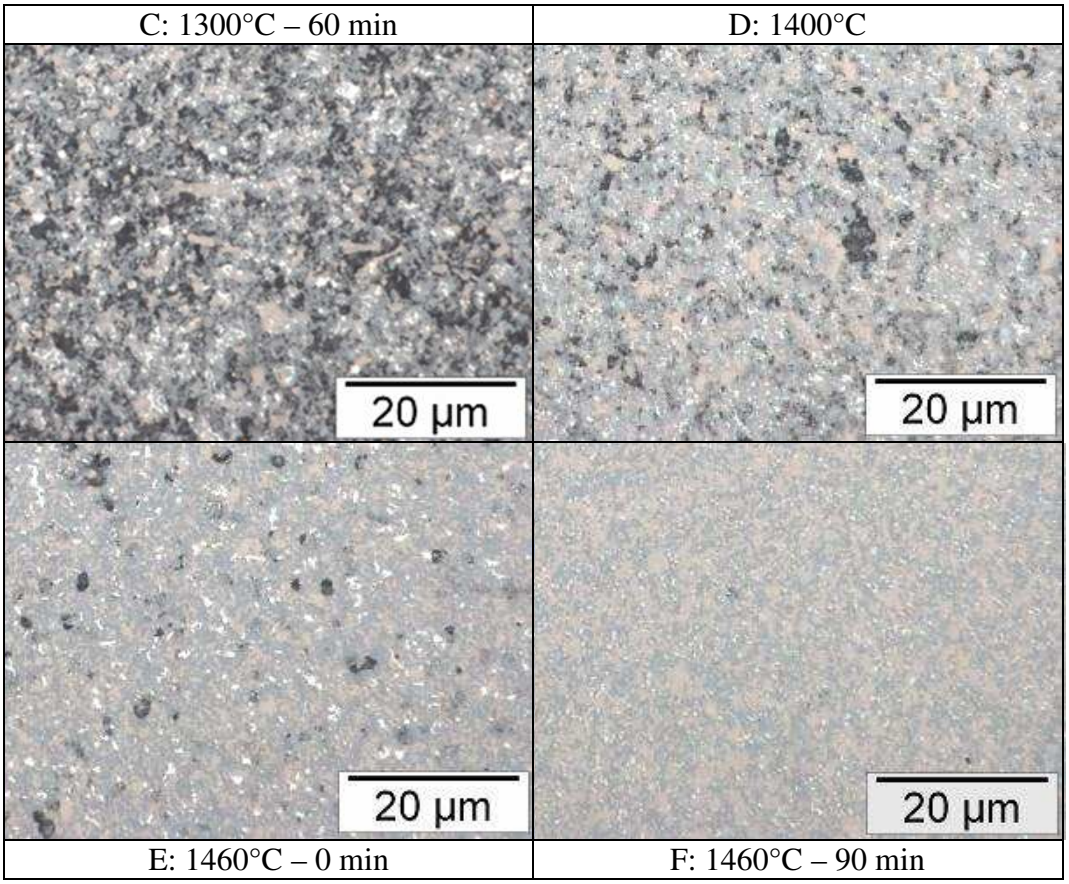

Figure 5. Microstructure evolution during sintering, cermet I

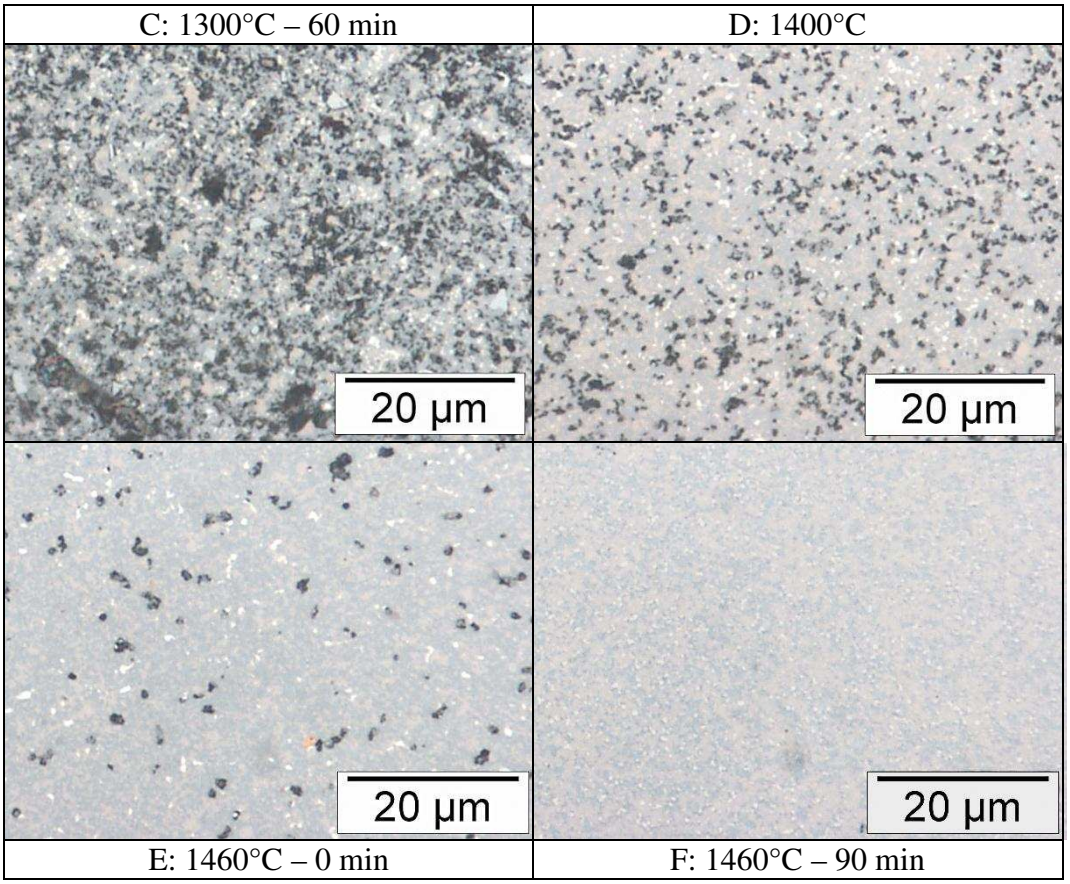

Figure 6. Microstructure evolution during sintering, cermet II

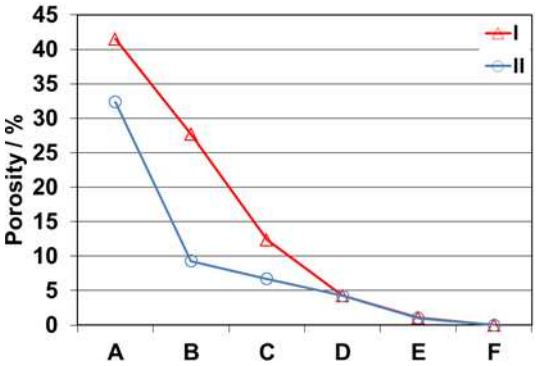

Figure 7. Porosity upon sintering for cermet I (with fine Ti(C,N)) and II (with submicron Ti(C,N))

Scanning electron microscopy

As Figure 8 and 9 show the evolution of the microstructure using a larger magnification of the SEM, several new features can be detected. At 1175°C (A) some binder pools are present. The homogenisation of the binder is first completed above 1400°C (D-F), which correlates with an increase of the shrinkage rate and the subsequent formation of the liquid phase (Figure 4).

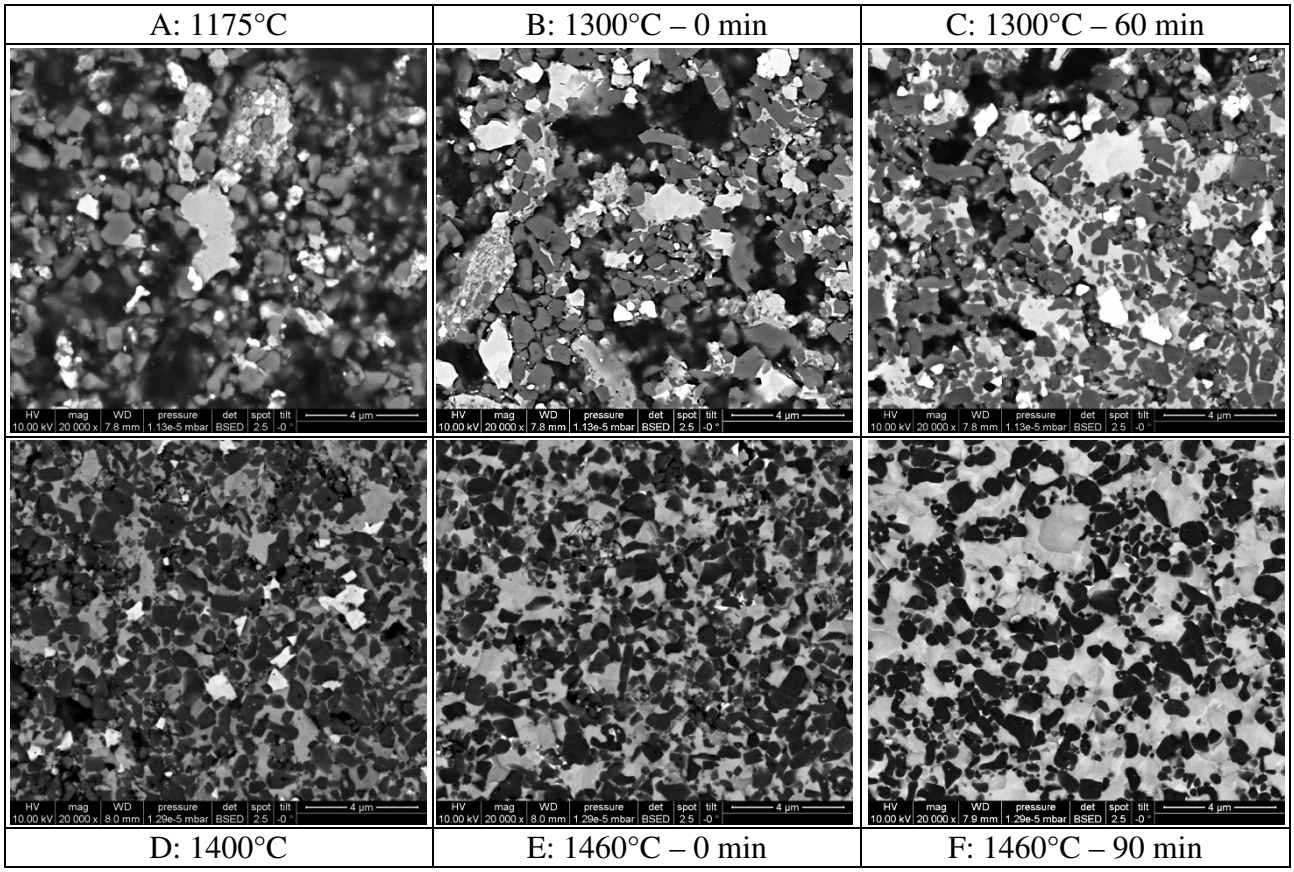

Figure 8. Microstructure evolution of cermet I (fine Ti(C,N)), SEM, BSE, 20000x

The Ti(C,N) particles (their comparatively low atomic number causes the particles to appear as almost black in back-scattered SEM-images) are present during the entire sintering cycle, although some dissolution takes place (Figure 8, 9). At stages where Ti(C,N) can be unambiguously identified (D to F) a much finer particle size is visible in cermet II. Image analysis reveals that the Ti(C,N) fraction decreases faster with submicron Ti(C,N) as for fine Ti(C,N) (Figure 10). This shows that the reactivity of submicron Ti(C,N) powder is larger than that of fine Ti(C,N) powder[2]. The WC fraction (the brightest particles in the back-scattered SEM-images) declines during sintering, while a homogenised outer rim phase composed of all elements except the binder phase (intermediate grey) is formed (Figure 8, 9 and 10). The hexagonal WC is dissolved in both cermet grades between stage D and E. Some inverse grains with bright core (W-rich) and darker rim (Ti-rich) are occasionally formed during the dwell time at 1460°C (F).

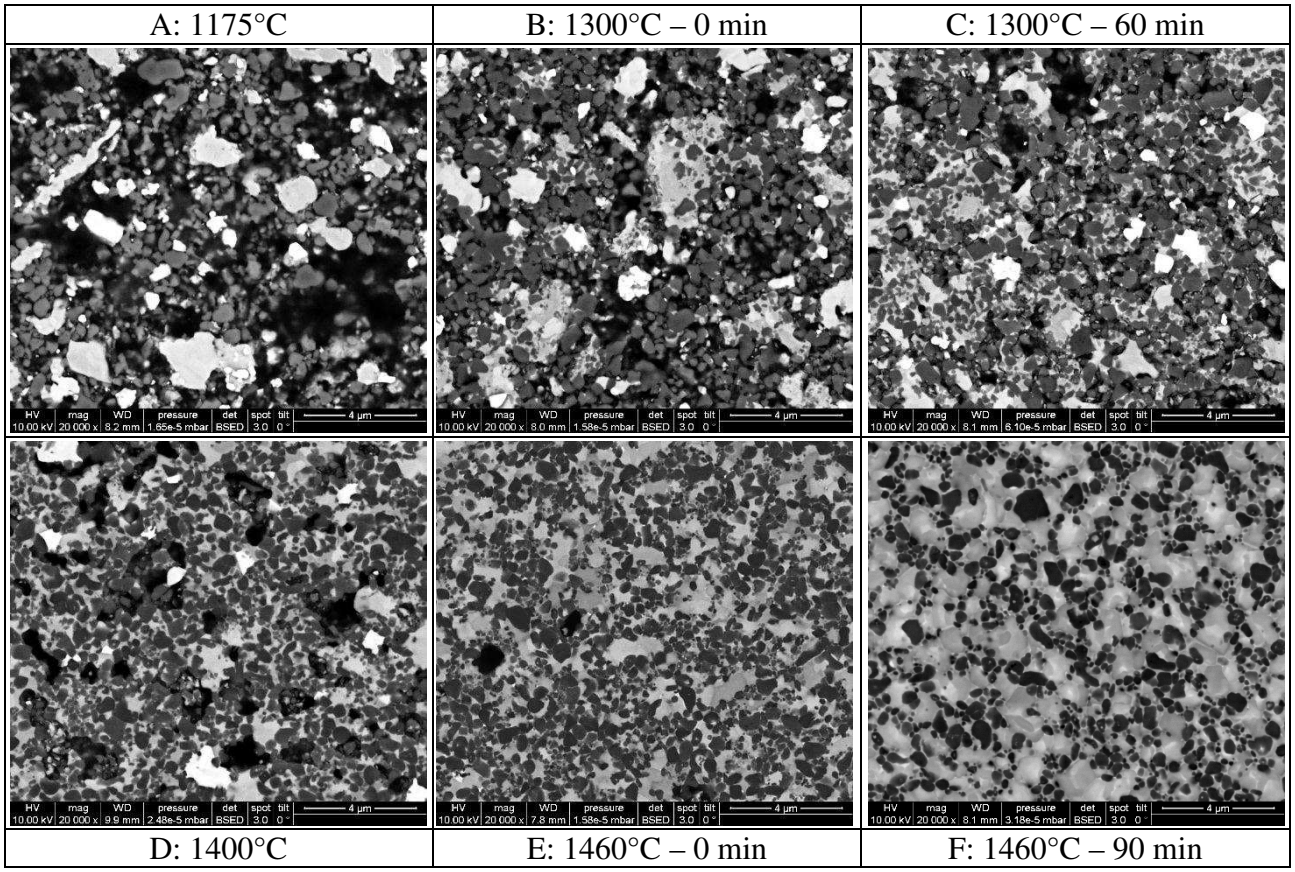

Figure 9. Microstructure evolution of cermet II (submicron Ti(C,N), SEM, BSE, 20000x

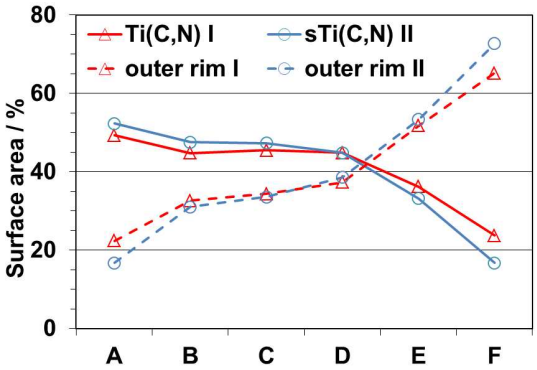

Figure 10. Surface area of Ti(C,N) core- (continuous line) and outer rim-phase (broken line) during sintering for cermet I (triangle) and II (circle)

Phase formation investigated by XRD

Figure 11 shows the XRD patterns of both cermets at the various stages of sintering (A-F). It is apparent, that for both cermets the (200) line of (Ta,Nb)C at 40.5° can only be identified at stage A (1175°C). At the next stage B (1300°C – 0 min) no more (Ta,Nb)C is present. Between 1175°C and 1300°C this phase homogenised with parts of Ti(C,N) to form a homogeneous fcc outer rim phase. At the formation temperature range between 1175 and 1300°C both cermets exhibit a large porosity, therefore their nitrogen activity is low[3] and the so-formed rim contains primarily a large amount of the metals Ti, Ta, Nb together with C. This multi-component rim phase has an increased lattice parameter as compared to Ti(C,N) (Table V). With increasing temperature a further dissolution of Ti(C,N) and WC leads to a decrease of the lattice parameter of the homogenised phase after stage D (Figure 12,

center). The intake of W,Ti and N, makes the lattice smaller and shifts the corresponding XRD-lines to larger diffraction angles (Figure 11). With increasing temperature and mainly in presence of liquid phase above 1400°C (D-F) the homogenisation increases, leading finally to an overlap of the diffraction lines of the homogenised outer rim phase with that of the remaining Ti(C,N) core.
Obviously, the lattice parameter of Ti(C,N) in cermet I remains constant during sintering, while in cermet II it increases slightly up to 1400°C. Supposing that Ta, Nb and W do not diffuse into the Ti(C,N) particles, it implies an increase of the [C]/[N] ratio, firstly by diffusion of dissolved C from the binder phase into Ti(C,N)[4] and secondly by outgassing of N_2[5]. During liquid-phase sintering, the lattice parameter of Ti(C,N) decreases for both grades because of the higher N-activity, leading to a lower [C]/[N] ratio. The higher reactivity of submicron Ti(C,N) leads to a larger decrease of the [C]/[N] ratio and therefore to a lower lattice parameter (Table IV, Figure 12, left). The lattice parameter of the binder phase changes dramatically from room temperature to 1175°C (Figure 12, right), after that it remains practically constant. The increase is primarily due to the dissolution of WC[6]and (Ta,Nb)C[7,8]. Afterwards, the lattice parameter of the binder for both cermets is nearly equal - slight variations are caused by different amounts of dissolved elements.

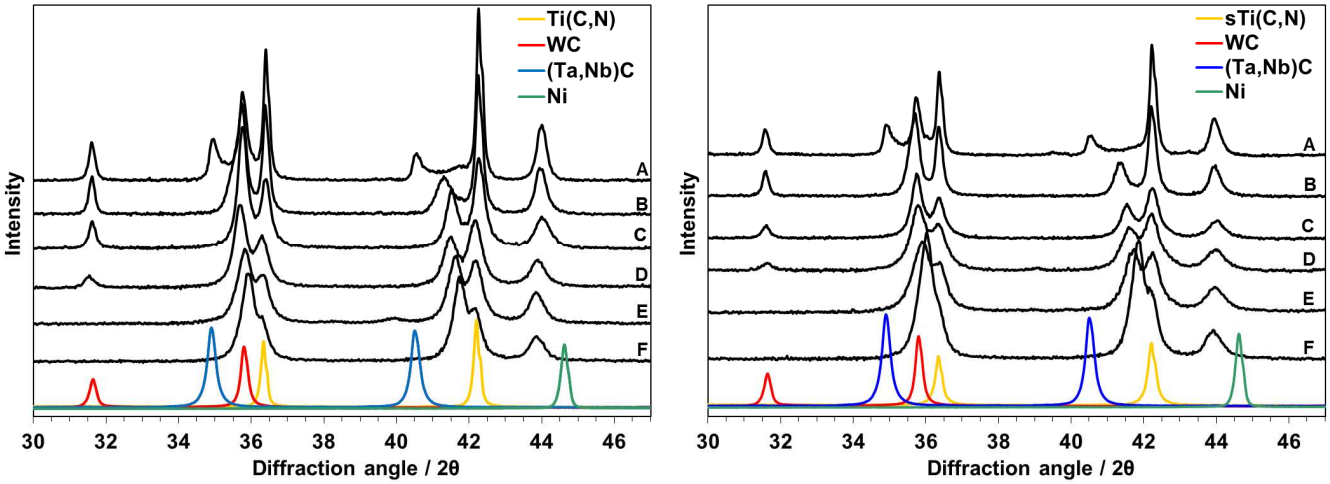

Figure 11. XRD patterns of cermet I (left) and II (right) after interrupted sintering compared with starting powders

Table V. Lattice parameters of Ti(C,N), binder and homogenised outer rim phase during sintering
*blend: binder phase from the lattice parameters of Co and Ni using Vegard's law

	Lattice parameter / Å					
	Core - Ti(C,N)		Outer rim phase		Binder phase	
	I	II	I	II	I	II
Blend	4.284	4.286	-	-	3.534*	3.534*
A: 1175°C	4.284	4.286	4.355	4.351	3.572	3.574
B: 1300°C – 0 min	4.284	4.285	4.378	4.372	3.573	3.572
C: 1300°C – 60 min	4.285	4.287	4.359	4.356	3.571	3.571
D: 1400°C	4.285	4.289	4.353	4.352	3.574	3.575
E: 1460°C – 0 min	4.284	4.287	4.341	4.343	3.577	3.575
F: 1460°C – 90 min	4.282	4.280	4.323	4.320	3.573	3.572

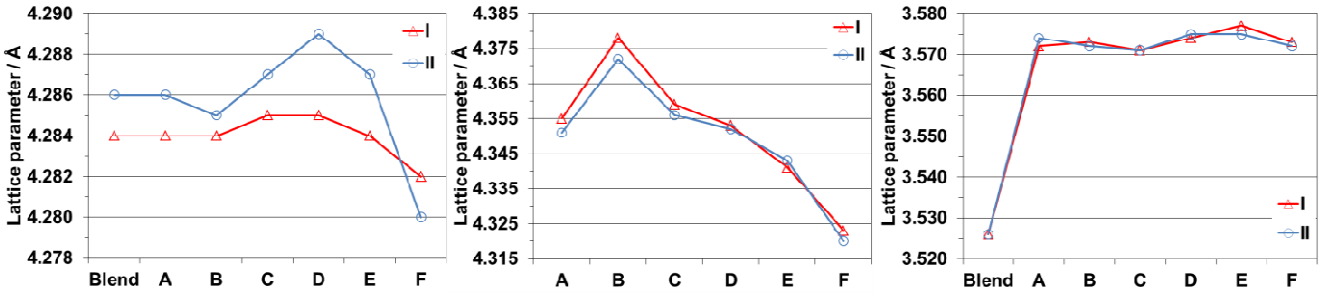

Figure 12. Lattice parameter of Ti(C,N) (left), the outer rim phase (center) and the binder phase (right)

Magnetic and mechanical properties

When interrupting the sintering process, it is assumed that the binder is not given enough time to change its composition due to the high cooling speed and that the magnetic properties remain constant.

After a significant increase of the magnetic saturation ($4\pi\sigma$) from stage A (1175°C – 90 min) to stage B (1300°C – 0 min), due to the formation of a binder phase skeleton, the magnetic saturation remains approximately constant (stage B to E) (Table VI, Figure 13). The slightly higher magnetic saturation of cermet II in stages C (1300°C – 60 min) to F (1460°C – 90 min) might originate in the lower amount of dissolved elements in the binder. The hard phase components show higher reactivity among themselves and therefore, a slightly lower dissolution in the binder than in cermet I[9]. This is in correspondence with the advanced formation of outer rim phase in cermet II, as compared to that of cermet I (Figure 10), which is especially true for the last step F (1460°C – 90 min). The increase in magnetic saturation at 1460°C from E (0 min) to F (90 min) is due to the redissolution of alloying elements, present in the binder phase, back into fcc-hard phase particles, aided by the presence of liquid phase.

The coercive force (HcJ) increases significantly from A (1175°C – 90 min) to D (1400°C), where the liquid phase is formed (Table VI, Figure 13). Then, it remains relatively stable at stages D (1400°C) to F (1460°C – 90 min). This stability of HcJ at high temperature is an indication of the stability of the hard phase and the absence of grain growth. Cermet II has a higher HcJ than cermet I due to the finer grain size of hard particles in cermet II.

The hardness (HV10) of cermet I and II after sintering is 1820 and 1850, while their fracture toughness (K_{IC}) is 8.0 and 7.5, respectively. Cermet II has a higher hardness since more fine Ti(C,N) particles remain in the final microstructure (Hall-Petch effect). Furthermore there is a larger amount of outer rim phase (Ti,W,Ta,Nb)(C,N) (25-26 GPa HV0.1)[10] present in Cermet II, which is harder than $Ti(C_{0.5}N_{0.5})$ (23 – 24 GPa HV0.1)[11] and which therefore increases the total hardness.

Table VI. Magnetic properties evolution during sintering

	$4\pi\sigma$ / $\mu T \cdot cm^3 \cdot kg^{-1}$		HcJ / $kA \cdot m^{-1}$	
	I	II	I	II
A: 1175°C	57.8	60.4	4.76	5.32
B: 1300°C - 0 min	98.8	96.3	12.37	14.56
C: 1300°C - 60 min	100.9	104.4	14.37	17.8
D: 1400°C	101.6	103.6	20.07	23.29
E: 1460°C - 0 min	100.0	104.9	18.48	23.43
F: 1460°C - 90 min	107.6	115.4	18.85	23.09

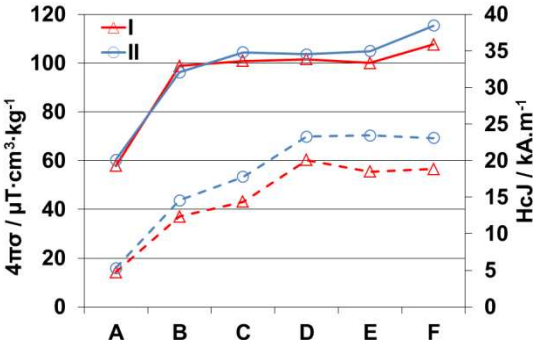

Figure 13. Magnetic saturation $4\pi\sigma$ (continuous line) and coercive force (broken line) of cermets I (triangle) and II (circle) during sintering

CONCLUSIONS

The current study highlights the effects of submicron Ti(C,N) powder in comparison with fine Ti(C,N) powder in the sintering process of Ti(C,N)-rich cermet alloys. Dilatometry experiments reveal a higher shrinkage during solid-state sintering for the cermet-grade containing submicron Ti(C,N) powder, because of the powders higher reactivity, while the total shrinkage after liquid-phase sintering remains unchanged. By interrupting the sintering cycles at various temperatures it was found that the more reactive submicron Ti(C,N) powder causes further dissolution of Ti(C,N) cores during liquid-phase sintering. Thus, a lower fraction of Ti(C,N) and a larger amount of a homogeneous outer rim phase, composed of dissolved elements, remain after sintering. A comparison of the cermets' magnetic properties confirm a smaller grain size of cermets made of submicron Ti(C,N) through all stages of sintering and a higher fraction of the homogeneous outer rim phase. This leads to a higher hardness of the cermet made from submicron Ti(C,N).

REFERENCES

[1]A. Demoly, W. Lengauer, C. Veitsch, K. Rabitsch, *Effect of submicron Ti(C,N) on the microstructure and the mechanical properties of Ti(C,N)-based cermets*, Int. J. Refract. Met. Hard Mater., **29**, 716-723 (2011).

[2]J. Jung, S. Kang, *Effect of ultra-fine powders on the microstructure of Ti(CN)–xWC–Ni cermets*, Acta Mater., **52**, 1379-1386 (2004).

[3]P. Lindahl, P. Gustafson, U. Rolander, L. Stals, H.-O. Andrén, *Microstructure of model cermets with high Mo or W content*, Int. J. Refract. Met. Hard Mater., **17**, 411-442 (1999).
[4]P. Ettmayer, H. Kolaska, W.Lengauer, K. Dreyer, *Ti(C,N) cermets – metallurgy and properties*, Int. J. Refract. Met. Hard Mater., **13**, 343-351 (1995).
[5]L. Chen, W. Lengauer, P. Ettmayer, K. Dreyer, H.W. Daub, D. Kassel, *Fundamentals of liquid phase sintering for modern cermets and functionally graded cemented carbonitrides (FGCC)*, Int. J. Refract. Met. Hard Mater., **18**, 307-322 (2000).
[6]J. Zackrisson, H.-O. Andrén, *Effect of carbon content on the microstructure and mechanical properties of (Ti,W,Ta,Mo)(C,N)–(Co,Ni) cermets*, Int. J. Refract. Met. Hard Mater., **17**, 265-273 (1999).
[7]H. Yoshimura, T. Sugizawa, K. Nishigaki, H. Doi, *Reaction occurring during sintering and the characteristics of TiC-20TiN-15WC-10TaC-9Mo-5.5Ni-11Co Cermet*, Int. J. Refract. Met. Hard Mater., **2**, 170-174 (1983).
[8]M. Qian, L.C. Lin, *On the disappearance of Mo2C during low temperature sintering of Ti(C,N)-Mo_2C-Ni cermets,* J. Mater. SCi. 34, 3677-3684 (1999).
[9]D.-G. Ahn, K.-W. Lee, J.-W. Lee, M. Sharon, *Study on magnetic-mechanical properties of Ti(C,N)-based cermet with sintering conditions*, Proc. WorldPM2004, Vienna (A), 537-542, EPMA, Shrewsbury, UK (2004).
[10]R. Königshofer, A. Liersch, W. Lengauer, T. Koch, M. Scheerer, W. Hohenauer, *Solid-state properties of binary, ternary and quaternary transition metal carbonitrides*, World PM2004, PM Tool Materials, Vienna, Vol. 3, 593-598 (2004).
[11]W. Lengauer, S. Binder, K. Aigner, P. Ettmayer, A. Guillou, J. Debuigne, G. Groboth, *Solid state properties of group IVb carbonitrides*, J. Alloys Comp. **217**, 137-147 (1995).